Materialia 22 (2022) 101426

Contents lists available at ScienceDirect

Materialia

journal homepage: www.elsevier.com/locate/mtla

A quantitative strategy for achieving the high thermal conductivity of die-cast Mg-Al-based alloys

Xixi Dong[a,*], Lingyun Feng[a], Shihao Wang[a], Feng Wang[b], Rohollah Ghasemi[c], Gang Ji[d], Eric A. Nyberg[e], Shouxun Ji[a,*]

[a] Brunel Centre for Advanced Solidification Technology (BCAST), Brunel University London, Uxbridge UB8 3PH, United Kingdom
[b] School of Metallurgy and Materials, University of Birmingham, Birmingham B15 2TT, United Kingdom
[c] Husqvarna AB, Drottninggatan 2, Huskvarna SE-561 82, Sweden
[d] Univ. Lille, CNRS, INRAE, Centrale Lille, UMR 8207 - UMET - Unité Matériaux et Transformations, Lille F-59000, France
[e] Kaiser Aluminum, Spokane Valley, WA 99216, United States

ARTICLE INFO

Keywords:
Magnesium alloys
Thermal conductivity
Microstructure
Mechanical property
Casting

ABSTRACT

A quantitative strategy was reported to design and develop Mg-Al-based alloys to achieve high thermal conductivity, in which the specific RE elements can be introduced to reduce the Al concentration in Mg matrix and to suppress the formation of $Mg_{17}Al_{12}$ phase through the formation of new intermetallic phases. Based on quantitative calculations, the strategy was demonstrated by a novel die-cast Mg3.2Al4.4La0.4Nd (in wt.%) alloy, which provided the thermal conductivity of 114.3 W/(m•K) at ambient temperature and 137.5 W/(m•K) at 300 °C, ~25% higher than the commercial Mg4Al4RE (AE44) alloy. Meanwhile, the alloy also offered excellent ambient yield strength of 143.2 MPa and elongation of 8.2%, and superior strength and ductility than the AE44 alloy at elevated temperatures.

1. Introduction

Magnesium (Mg) alloys have been becoming significantly attractive as light-weight structural materials in the past few decades [1,2]. In competing with aluminium (Al) alloys, Mg alloys have advantages of low density, high strength ratio, and better electromagnetic shielding properties and castability [2,3]. However, Mg alloys usually have inferior thermal conductivity to their competitive Al alloys. Therefore, it is essential for Mg alloys to have improved thermal conductivity. This is particularly important for recent developments of high thermal conductivity die-cast Mg alloys to replace relevant aluminium alloys, for the deep lightweight and heat transfer requirements in emerging applications including engines in drones and handheld powered tools, and electric motors and battery packs in electric and unmanned aerial vehicles [3–5].

Aluminium (Al) is a popular and key alloying element in cast Mg alloys for improving castability and ambient mechanical properties. The majority of commercially available die-cast Mg alloys are based on Mg-Al alloy systems [6,7]. However, the die-cast Mg-Al-based alloys usually have poor thermal conductivity. The thermal conductivity of typical AZ91D, AM60 and AM50 alloys for low temperature applications is 51, 61 and 65 W/(m•K) at room temperature (RT) [8], and that of the typical MRI153M, MRI230D, AJ62, AS21, AE42 and AE44 alloys for elevated applications is 64, 77, 77, 84, 84 and 85 W/(m•K) [8,9], respectively. Various effects on the thermal conductivity of Mg alloys have been investigated including solid solution [10–12], secondary phase [12,13], heat treatment [14,15], deformation [16] and temperatures [17]. The solid solution of solute atoms into Mg matrix was thought to be the most detrimental factor for the thermal conductivity of Mg alloys [3,12]. In detail, solute atoms induced lattice distortion and shortened the mean free path of the phonons and electrons that were unbeneficial to heat transfer [3]. Therefore, the control of interaction of Al solute with Mg matrix can be an effective approach to improve the thermal conductivity of Mg-Al-based alloys without sacrificing the advantages in castability and mechanical properties. However, limited information for a quantitative strategy has been reported.

In this paper, we report a quantitative strategy in alloy design to improve the thermal conductivity of Mg-Al-based alloys. The verification using a demonstration alloy was introduced on alloy composition, casting, microstructure, thermal conductivity and mechanical properties at ambient and elevated temperatures. The novel intermetallic phases formed in the demonstration alloy were also investigated.

* Corresponding authors.
E-mail addresses: xixi.dong@brunel.ac.uk (X. Dong), shouxun.ji@brunel.ac.uk (S. Ji).

https://doi.org/10.1016/j.mtla.2022.101426
Received 26 March 2022; Accepted 9 April 2022
Available online 10 April 2022

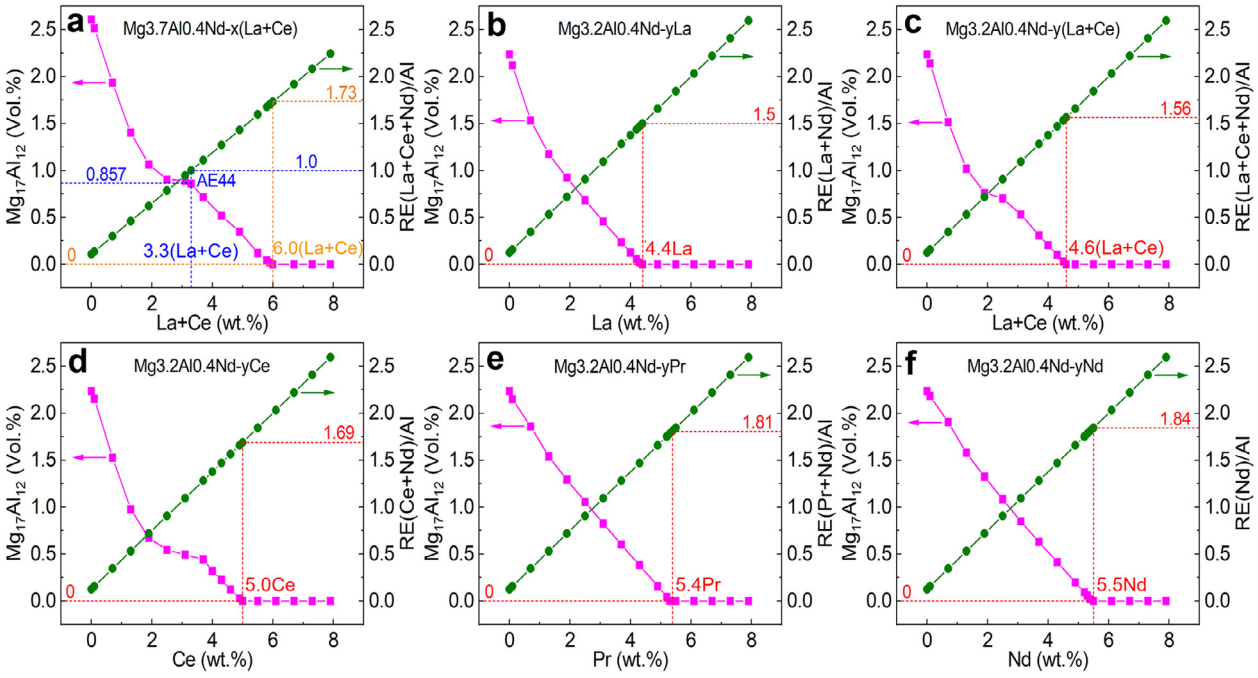

Fig. 1. Non-equilibrium calculation using Scheil model in Pandat CALPHAD software for the volume percentage of $Mg_{17}Al_{12}$ phase in (a) Mg3.7Al0.4Nd-x(La+Ce) AE44 type alloy, and the effect of RE contents of (b) La, (c) La+Ce mischmetal, (d) Ce, (e) Pr and (f) Nd on the formation of $Mg_{17}Al_{12}$ phase in the Mg3.2Al0.4Nd-yRE alloy.

2. Quantitative strategy

2.1. Proposal of design criteria

To maintain the castability and mechanical properties of Mg-Al based alloys, the Al content needs to set at a certain level. But the concentration of Al solute needs to be minimised in solution for least lattice distortion to improve thermal conductivity. Therefore, Al should be presented in a way to satisfy these conflict requirements in Mg-Al alloys. Generally, the specific Al solute in solution can be reduced by adding other solutes in solution that reduce the solid solubility of Al, or by changing the phase equilibria so that a different phase is in equilibrium with the matrix to lower the Al solute in solution. The solubility of Al in Mg is 12.7 wt.% [18]. The Al forms solution in Mg alloys and excessive Al solute can lead to the formation of $Mg_{17}Al_{12}$ intermetallic phase [7]. To improve the thermal conductivity, one or more elements can be introduced into Mg-Al system. The new elements should have higher affinity to Al and lower solubility in Mg, which can minimise the solubility of Al in Mg and form new phases to destabilize $Mg_{17}Al_{12}$ phase. Rare earth (RE) elements such as La, Ce, Pr and Nd can be the good candidates because the solubility of La, Ce, Pr and Nd in Mg is 0.23, 0.74, 1.7 and 3.6 (in wt.%), respectively [18–20]. More importantly, these RE elements can form Al-RE-based phases [21,22], which can suppress the formation of $Mg_{17}Al_{12}$ phase, as the affinity of RE-Al is higher than that of Mg-Al [7,23]. The improved thermal conductivity in AE44 alloy is the technical evidence in this regard, although limited quantitative analysis is disclosed to help us understand the underlying mechanism.

Based on these principles, to develop a quantitative strategy for die-cast Mg-Al-based alloys with high thermal conductivity, three criteria are set for element selection: (a) higher affinity with Al than Mg to reduce the concentration of Al solute in Mg matrix; (b) low solubility (< 5 wt.%) in Mg to reduce the solute concentration in Mg matrix; (c) $Mg_{17}Al_{12}$ phase is completely suppressed or replaced. The multicomponent calculation of phase diagrams (CALPHAD) can be used for quantitative thermodynamic evaluation.

2.2. Thermodynamic calculation

The most common RE elements of La, Ce, Pr and Nd were selected to verify the proposed quantitative strategy and non-equilibrium Scheil model was used to calculate phase formation during die-casting. Fig. 1a shows the calculation results for the $Mg_{17}Al_{12}$ phase formed during the solidification of Mg3.7Al0.4Nd-x(La+Ce) alloys that commercial AE44 alloy belongs to. The amount of $Mg_{17}Al_{12}$ phase decreases with the increase of La+Ce mischmetal when the Ce/La weight ratio is set as 2. The volume of $Mg_{17}Al_{12}$ phase approaches to zero when the La+Ce is 6 wt.%, where the weight ratio of RE(La+Ce+Nd)/Al is 1.73. At this point, the formation of $Mg_{17}Al_{12}$ phase is fully suppressed and Al solute should be minimised in Mg solution. However, when examining the AE44 alloy with the typical composition, the RE(La+Ce+Nd)/Al weight ratio is 1.0 and the calculated volume of $Mg_{17}Al_{12}$ phase is 0.857%, indicating a high level of Al in Mg matrix. The same method is applied to Mg3.2Al0.4Nd-yRE alloys using different RE elements and the results is shown in Figs. 1b-f. The optimized content was found to be 4.4 wt.% La, 4.6 wt.% La+Ce mischmetal, 5.0 wt.% Ce, 5.4 wt.% Pr or 5.5 wt.% Nd for completely supressing the formation of $Mg_{17}Al_{12}$ phase. Obviously, the singular addition of La has advantage as La is cheaper than Pr and Nd and the required amount for La is lower than Ce and Ce+La mixture. For the Mg3.7Al0.4Nd-x(La+Ce) AE44 type alloy, it requires 6.0 wt.% (La+Ce) to reach an optimized high thermal conductivity (Fig. 1a), which is much higher than the 3.3 wt.% (La+Ce) in the AE44 alloy, and this is industrially unacceptable in consideration of material cost. Therefore, the Mg3.2Al0.4Nd-yRE alloy was chosen as demonstration to verify the proposed strategy, as it only requires 4.4 wt.% La (Fig. 1b) and 2.7% increase in raw material cost (Supplementary Table S3), to reach the optimized high thermal conductivity (Fig. 2).

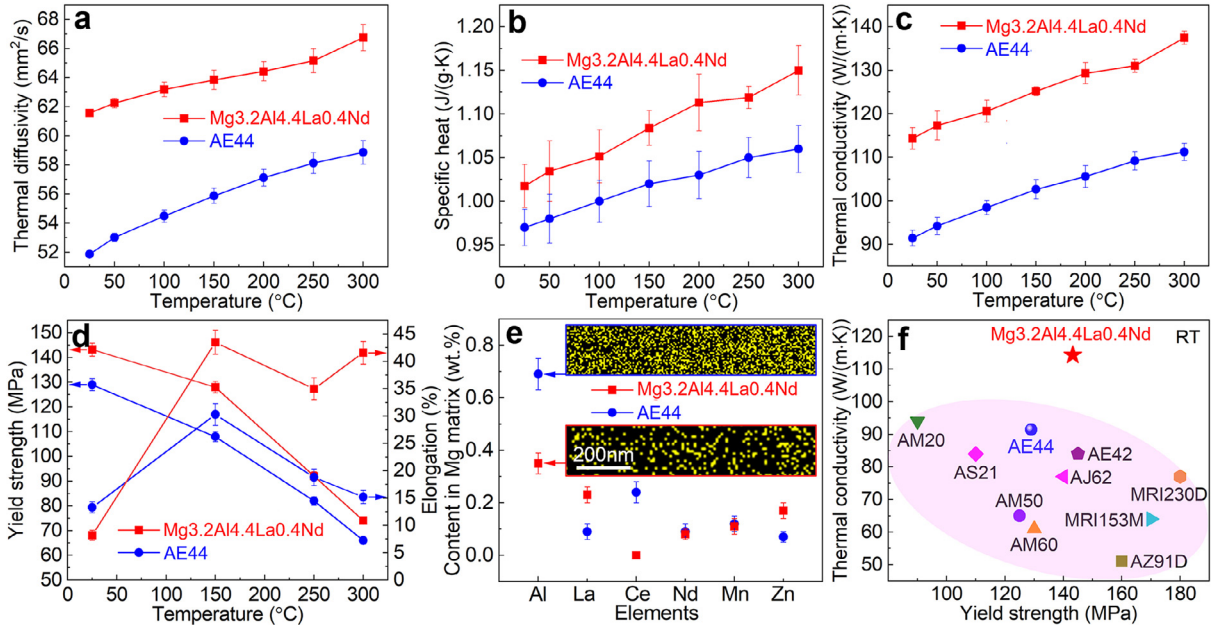

Fig. 2. (a) Thermal diffusivity, (b) specific heat, (c) thermal conductivity and (d) tensile properties of the Mg3.2Al4.4La0.4Nd alloy from room temperature up to the temperature of 300 °C, in comparison with the AE44 alloy. (e) STEM-EDS results for the solute contents of different elements in the Mg matrix of the Mg3.2Al4.4La0.4Nd and AE44 alloys. (d) Comparison of the thermal conductivity at room temperature of the Mg3.2Al4.4La0.4Nd alloy with commercial die-cast Mg alloys.

3. Experimental

3.1. Material preparation and die casting

In experiments, the master alloys were melted in a steel crucible with gas protection and the melts were held at 720 °C for 30 min before casting using a cold-chamber high pressure die casting. Each shot consisted of eight standard Ø6.35 mm cylindrical samples [4] for tensile tests and one 4 mm thickness plate for thermal conductivity measurements. The die was preheated to 230 °C and the intensification pressure was 320 bar. The composition of the demonstration alloy was measured as Mg3.2Al4.4La0.4Nd0.2Zn0.2Mn (denoted as Mg3.2Al4.4La0.4Nd) by ICP-AES. Commercial AE44 alloy with the composition of Mg3.7Al1.1La2.2Ce0.4Nd0.1Zn0.2Mn (denoted as AE44) was used for comparison.

3.2. Thermal conductivity measurement

The thermal conductivity λ is determined by $\lambda = \alpha * C_p * \rho$, in which α is the thermal diffusivity, Cp is the specific heat and ρ is the density [3]. The thermal diffusivity was measured by the laser-flash method using a Netzsch LFA-427, and the specific heat was measured on a Netzsch 404C differential scanning calorimetry. The density was measured using the Archimedes method, and the change of density at elevated temperatures was determined by measuring the thermal expansion using a Shimadzu TMA-50.

3.3. Tensile tests and characterisation

Tensile tests were performed using an Instron 5500 Testing System, and the ramp rates for the RT and elevated tensile tests were 1 mm/min and 0.0002/s, respectively. The gauge size of the cylindrical tensile samples was Ø6.35 × 50 mm. An Instron STATIC type extensometer with the gauge length of 50 mm was applied during RT tensile tests, and no extensometer was used during elevated tensile tests. Each reported data was based on the measurement of at least 8 samples. Microstructures were characterized on a Zeiss SUPRA-35VP scanning electron microscope (SEM) and a FEI Tecnai G2 transmission electron microscope (TEM), including bright-field imaging, selected area electron diffraction (SAED), scanning transmission electron microscopy (STEM) imaging and energy dispersive X-ray spectroscopy (EDS) mapping under STEM mode.

4. Results and discussion

4.1. Thermal and mechanical properties

Figs. 2a-d shows the measurement of the thermal diffusivity, specific heat, thermal conductivity and tensile properties of the die-cast Mg3.2Al4.4La0.4Nd and AE44 alloys from RT up to 300 °C, respectively. The measurement of the density and ultimate tensile strength (UTS) are provided in Supplementary Fig. S1 and the tensile curves are provided in Supplementary Fig. S2. With the increase of the temperature from RT to 300 °C, the thermal diffusivity increased from 61.5 to 67.7 mm^2/s, the specific heat increased from 1.02 to 1.15 J/(g•K), the density decreased from 1.825 to 1.791 g/cm^3. Therefore, the thermal conductivity increased from 114.3 to 137.5 W/(m•K). Moreover, in the same temperature range, the yield strength decreased from 143 to 74 MPa, the UTS decreased from 244 to 80 MPa, but the elongation increased from 8.2% to 41.6%. Comparing with the AE44 alloy for the properties at RT, the thermal diffusivity, specific heat, density, thermal conductivity and yield strength of the Mg3.2Al4.4La0.4Nd alloy were improved by 18.7%, 4.9%, 0.5%, 25% and 11%, respectively. Clearly, the improvement of the thermal diffusivity was the main reason for the increase of the thermal conductivity, due to the efficient suppression of the solution concentration of Al in the Mg matrix from 0.69 wt.% to 0.35 wt.% (Fig. 2e, Supplementary Fig. S3 and Table S1). In comparison with the AE44 alloy, the normalized ratio between the Al concentration in Mg matrix and the Al addition in the Mg3.2Al4.4La0.4Nd alloy decreased significantly from 18.65% to 10.94%, i.e., a 41% decrease in the solution ratio of Al in Mg matrix, which showed the effectiveness of the optimized addition of RE for the decrease of Al concentration in Mg matrix.

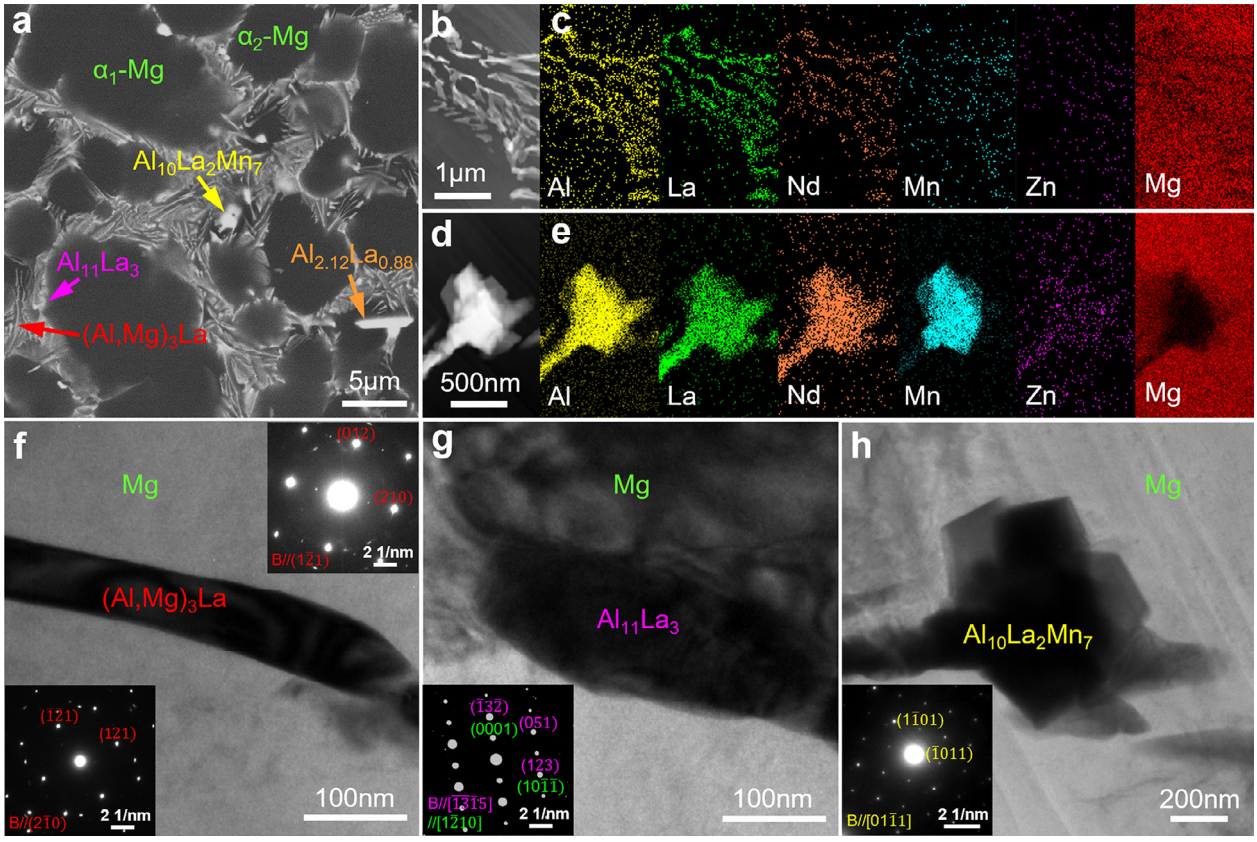

Fig. 3. Microstructure of the Mg3.2Al4.4La0.4Nd alloy under as-cast condition. (a) Backscattered SEM image; (b) STEM image of the $(Al,Mg)_3La$ and $Al_{11}La_3$ phases at GBs; (c) STEM-EDS mapping showing the elemental distributions in (b); (d) STEM image of the $Al_{10}La_2Mn_7$ phase at GBs; (e) STEM-EDS mapping showing the elemental distributions in (d). Bright-field TEM images and the corresponding SAED patterns confirming the (f) $(Al,Mg)_3La$, (g) $Al_{11}La_3$ and (h) $Al_{10}La_2Mn_7$ phases.

Compared to the AE44 alloy at elevated temperatures, the Mg3.2Al4.4La0.4Nd alloy showed the similar level of increase in the density, thermal conductivity and yield strength as that at RT, except that the improvement of thermal diffusivity decreased and the improvement of specific heat increased, as shown in Fig. 2 and Supplementary Table S2. Furthermore, the comparison with the AE44 alloy in Supplementary Table S3 indicated that the raw material cost in the Mg3.2Al4.4La0.4Nd alloy only increased by 2.7%. From Fig. 2f, the Mg3.2Al4.4La0.4Nd alloy has significant advantage in the thermal conductivity over the existing commercial die-cast Mg alloys. Also, it confirmed that the demonstration alloy delivers good strength. Overall, these results have validated the success of proposed strategy.

4.2. Novel $(Al,Mg)_3La$ intermetallic phase

In the AE44 alloy, it was reported that $Al_{11}RE_3$ was predominant phase, Al_2RE was minor phase, and $Al_{10}RE_2Mn_7$ phase was occasionally detected [21,24,25]. Fig. 3 shows the microstructure of the Mg3.2Al4.4La0.4Nd alloy under as-cast condition. Typically, a bimodal distribution [4] of α-Mg phase was observed. However, different from the AE44 alloy, a novel lamellar and fibrous $(Al,Mg)_3RE$ phase replaced $Al_{11}RE_3$ as the predominant intermetallic phase and $Al_{11}RE_3$ degraded to the minor intermetallic phase, and interestingly another novel $Al_{2.12}RE_{0.88}$ phase was detected as the second minor intermetallic phase, while the blocky $Al_{10}RE_2Mn_7$ phase was also occasionally found in the Mg3.2Al4.4La0.4Nd alloy (Fig. 3a).

To confirm intermetallic phase, SAED was conducted on at least three particles and at least two zone axes for each particle. Two SAED patterns are provided for the novel $(Al,Mg)_3RE$ phase (Fig. 3f), which agrees with the $(Al,Mg)_3La$ phase (Orthorhombic, a = 4.336 Å, b = 18.867 Å, c = 4.424 Å, Space group: $C222_1$ [26]). The $(Al,Mg)_3La$ phase was also observed recently in a gravity cast Mg-4.5Al-6.3La alloy [27]. The SAED pattern of the $Al_{11}RE_3$ phase (Fig. 3g) fits the $Al_{11}La_3$ phase (Orthorhombic, a = 4.431 Å, b = 13.142 Å, c = 10.132 Å, Space group: *Immm* [27]), while the SAED pattern of the $Al_{10}RE_2Mn_7$ phase (Fig. 3h) agrees with the $Al_{10}La_2Mn_7$ phase (Hexagonal, $a = b$ = 9.049 Å, c = 13.21 Å, Space group: R-3 m [22,28]), and one SAED pattern is provided for clarity as these two phases were well identified [21,28] in the AE series Mg alloys. Figs. 3c&e showed that $(Al,Mg)_3La$ mainly contains Al, Mg, La and Nd with a minor doping of Mn, and $Al_{10}La_2Mn_7$ mainly contains Al, La, Nd and Mn with a minor doping of Zn. Importantly, Nd could replace La without changing the crystal structure. It should be emphasized that the contrast difference of Mg in Figs. 3c&e confirmed the considerable presence of Mg in $(Al,Mg)_3La$, which is clearly a novel phase that has a different crystal structure from the Al_3La phase. According to the composition analysis result in Supplementary Fig. S4, $(Al,Mg)_3La$ can be written as $Al_{1.46}Mg_{1.54}La_{0.89}Nd_{0.11}Mn_{0.06}Zn_{0.07}$.

4.3. Morphology of novel $Al_{2.12}RE_{0.88}$ phase

It is interesting to investigate the morphology of the novel $Al_{2.12}RE_{0.88}$ phase observed in the Mg3.2Al4.4La0.4Nd alloy, which has been seldomly reported. Fig. 4 showed the STEM-EDS mapping and SAED results for the longitudinal and cross-sectional morphology of the $Al_{2.12}RE_{0.88}$ phase. The SAED pattern under the projection direction of $[\bar{1}101]$ (Fig. 4c) fits the $Al_{2.12}La_{0.88}$ phase (Hexagonal, a=b=4.382 Å, c=4.349 Å, Space group: *P6/mmm* [26]). The SAED pattern under the projection direction of $[\bar{1}\bar{1}23]$ (Fig. 4g) also agrees with the $Al_{2.12}La_{0.88}$ phase. Under this zone axis, the characteristic truncated facets of $\{10\bar{1}0\}$ and $\{10\bar{1}1\}$ were identified, and the absence of $\{11\bar{2}0\}$ facets was suggested by the continuous edge profile. Combing the morphology in Fig 4c, $Al_{2.12}La_{0.88}$ owns a shape truncated by $\{10\bar{1}0\}$, $\{10\bar{1}1\}$, $\{11\bar{2}0\}$

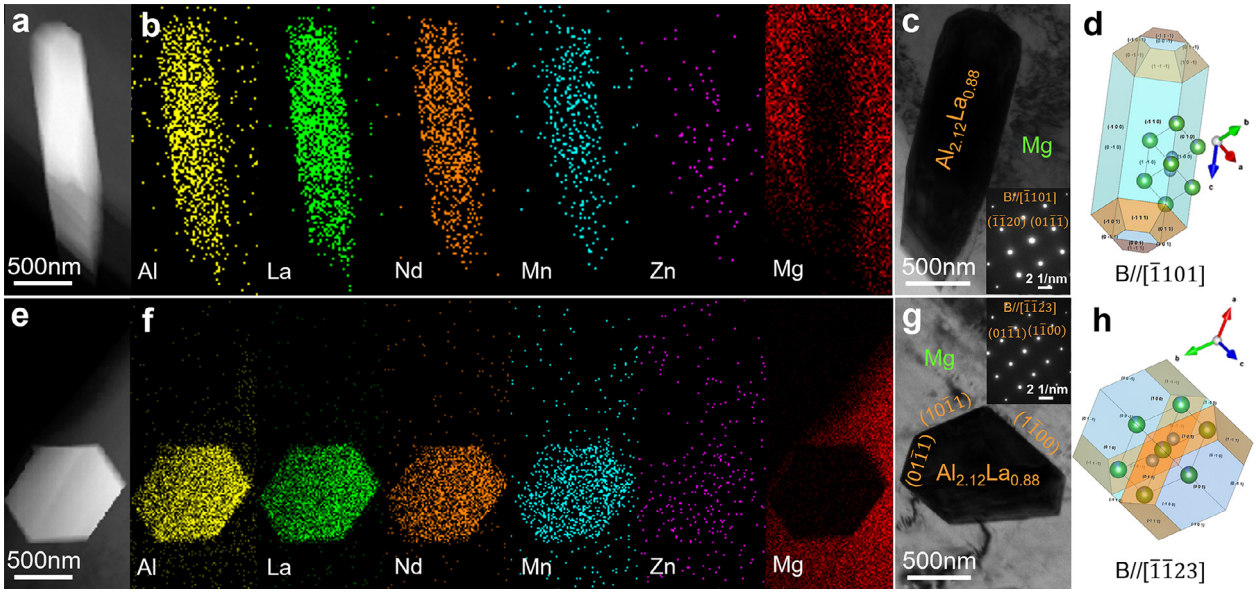

Fig. 4. Microstructure of the $Al_{2.12}La_{0.88}$ phase in the Mg3.2Al4.4La0.4Nd alloy under as-cast condition. Longitudinal view of $Al_{2.12}La_{0.88}$: (a) STEM image, (b) corresponding STEM-EDS mapping, (c) bright-field TEM image under the projection direction of [$\bar{1}$101] and corresponding SAED pattern, and (d) schematic showing the shape of $Al_{2.12}La_{0.88}$ in (c). Cross-sectional view of $Al_{2.12}La_{0.88}$: (e) STEM image, (f) corresponding STEM-EDS mapping, (g) bright-field TEM image under the projection direction of [$\bar{1}\bar{1}$23] and corresponding SAED pattern, and (h) schematic showing the shape of $Al_{2.12}La_{0.88}$ in (g).

and {0001}. Their shapes are schematically presented in Figs. 4d&h, where the preferential truncation of {10$\bar{1}$0} results in the elongated shape in Fig. 4c. Therefore, the truncation feature of $Al_{2.12}La_{0.88}$ is verified, while the 3D morphology of $Al_{2.12}La_{0.88}$ depends on the competitions between different truncated facets. The major elements in $Al_{2.12}La_{0.88}$ are Al, La, Nd and Mn with a minor doping of Zn. Nd could replace the atomic position of La without changing the crystal structure of $Al_{2.12}La_{0.88}$.

4.4. Discussion on thermal and mechanical properties

As shown in Supplementary Figs. S4 & S5, Tables S4& S5, the composition and content of the $(Al,Mg)_3RE$ phase at GBs of the Mg3.2Al4.4La0.4Nd alloy and the $Al_{11}RE_3$ phase at GBs of the AE44 alloy are similar. In addition, both $(Al,Mg)_3RE$ and $Al_{11}RE_3$ have orthorhombic crystal structure. These indicate the predominant formation of $(Al,Mg)_3RE$ has very limited effect on the improvement of the heat transfer at GBs. Furthermore, the misfit analysis between $(Al,Mg)_3RE/Al_{11}RE_3/Mg_{17}Al_{12}$ and Mg in Supplementary Tables S6, S7 and S8 shows that the predominant formation of $(Al,Mg)_3RE$ does not further decrease the misfit or improve the heat transfer between the major intermetallic phase at GBs and the Mg matrix. Moreover, it was well reported that the reduction of the thermal conductivity by the solid solution of 1 at.% solute atoms in the Mg matrix was 6.5~17.9 times higher than that by the formation of the corresponding intermetallic phase at GBs [29], and the solid solution of solute atoms in the Mg matrix was generally considered as the major factor for the control of the thermal conductivity [3,12]. Therefore, the predominant formation of $(Al,Mg)_3RE$ at GBs of the Mg3.2Al4.4La0.4Nd alloy should have very limited effect on the improvement of the thermal conductivity, and the remarkable improvement of the thermal conductivity in the Mg3.2Al4.4La0.4Nd alloy can be mainly attributed to the reduction of the Al concentration of in the Mg matrix and the complete suppression of $Mg_{17}Al_{12}$ phase, in contrast to the AE44 alloy. The enhanced strength especially at elevated temperatures can be attributed to the increased content of La, the complete suppression of the low melting-point $Mg_{17}Al_{12}$ phase [7,21] and the predominant formation of the $(Al,Mg)_3RE$ phase with slightly higher RE content and area fraction (Supplementary Tables S4& S5).

Conclusion

In summary, a quantitative strategy has been developed for Mg-Al based alloys to achieve high thermal conductivity, the specific RE elements can be introduced to reduce the Al concentration in Mg matrix and to suppress the formation of $Mg_{17}Al_{12}$ phase through the formation of new intermetallic phase. The demonstration using a La enriched die-cast Mg3.2Al4.4La0.4Nd alloy has successfully provided the excellent thermal conductivity of 114.3 W/(m•K) at RT and 137.5 W/(m•K) at 300 °C, which are remarkably (~25%) higher than the commercially popular AE44 alloy. Meanwhile, the alloy also offers excellent yield strength of 143.2 MPa and elongation of 8.2% at RT, and superior strength and ductility than the AE44 alloy at elevated temperatures. Interestingly, different from the predominant $Al_{11}RE_3$ intermetallic phases in the AE44 alloy, a novel lamellar and fibrous $(Al,Mg)_3RE$ phase and a hexagonal $Al_{2.12}RE_{0.88}$ phase are formed in the Mg3.2Al4.4La0.4Nd alloy.

Declaration of interest statement

The authors declare no competing interests for the manuscript “A quantitative strategy for achieving the high thermal conductivity of die-cast Mg-Al-based alloys” submitted to *Materialia*.

Supplementary materials

Supplementary material associated with this article can be found in the appendix.

Declaration of Competing Interest

The authors declare that they have no known competing financial interests or personal relationships that could have appeared to influence the work reported in this paper.

Acknowledgements

Financial supports from Innovate UK (Project reference: 10004694) and Husqvarna Group are gratefully acknowledged. Mr. Jon Gadd from BCAST helped in the die casting.

Supplementary materials

Supplementary material associated with this article can be found, in the online version, at doi:10.1016/j.mtla.2022.101426.

References

[1] T.M. Pollock, Weight loss with magnesium alloys, Science 328 (2010) 986–987.
[2] J. Hofstetter, S. Rueedi, I. Baumgartner, H. Kilian, B. Mingler, E. Povoden-Karadeniz, S. Pogatscher, P.J. Uggowitzer, J.F. Loeffler, Processing and microstructure–property relations of high-strength low-alloy (HSLA) Mg–Zn–Ca alloys, Acta Mater. 98 (2015) 423–432.
[3] S.B. Li, X.Y. Yang, J.T. Hou, W.B. Du, A review on thermal conductivity of magnesium and its alloys, J. Magnes. Alloy. 8 (2020) 78–90.
[4] X.X. Dong, L.Y. Feng, S.H. Wang, E.A. Nyberg, S. Ji, A new die-cast magnesium alloy for applications at higher elevated temperatures of 200–300°C, J. Magnes. Alloy. 9 (2021) 90–101.
[5] X.X. Dong, S. Ji, A casting magnesium alloy for providing improved thermal conductivity, WIPO Patent (2020) WO2020221752A1.
[6] A.A. Luo, Magnesium casting technology for structural applications, J. Magnes. Alloy. 1 (2013) 2–22.
[7] M. Pekguleryuz, M. Celikin, Creep resistance in magnesium alloys, Int. Mater. Rev. 55 (2010) 197–217.
[8] https://www.meridian-mag.com/magnesium-die-casting/lightweight-alloys/datasheet.pdf.
[9] A. Rudajevová, P. Lukáč, Comparison of the thermal properties of AM20 and AS21 magnesium alloys, Mater. Sci. Eng. A 397 (2005) 16–21.
[10] H. Pan, F. Pan, R. Yang, J. Peng, C. Zhao, J. She, Z. Gao, A. Tang, Thermal and electrical conductivity of binary magnesium alloys, J. Mater. Sci. 49 (2014) 3107–3124.
[11] L. Zhong, J. Peng, S. Sun, Y. Wang, Y. Lu, F. Pan, Microstructure and thermal conductivity of as-cast and as-solutionized Mg–rare earth binary alloys, J. Mater. Sci. Technol. 33 (2017) 1240–1248.
[12] C. Su, D. Li, A. Luo, T. Ying, X. Zeng, Effect of solute atoms and second phases on the thermal conductivity of Mg-RE alloys: a quantitative study, J. Alloy. Compd. 747 (2018) 431–437.
[13] Y.F. Liu, X.J. Jia, X.G. Qiao, S.W. Xu, M.Y. Zheng, Effect of La content on microstructure, thermal conductivity and mechanical properties of Mg–4Al magnesium alloys, J. Alloy. Compd. 806 (2019) 71–78.
[14] C. Wang, Z. Cui, H. Liu, Y. Chen, W. Ding, S. Xiao, Electrical and thermal conductivity in Mg–5Sn Alloy at different aging status, Mater. Des. 84 (2015) 48–52.
[15] R.N. Lumley, I.J. Polmear, H. Groot, J. Ferrier, Thermal characteristics of heat-treated aluminum high-pressure die-castings, Scr. Mater. 58 (2008) 1006–1009.
[16] L. Zhong, J. Peng, Y. Sun, Y. Wang, Y. Lu, F. Pan, Microstructure and thermal conductivity of as-cast and as-extruded binary Mg–Mn alloys, Mater. Sci. Technol. 33 (2017) 92–97.
[17] S. Lee, H.J. Ham, S.Y. Kwon, S.W. Kim, C.M. Suh, Thermal conductivity of magnesium alloys in the temperature range from −125°C to 400°C, Int. J. Thermophys. 34 (2013) 2343–2350.
[18] H. Okamoto, La-Mg (Lanthanum-Magnesium), J. Phase Equilib. 34 (2013) 161–162.
[19] A.A. Nayeb-Hashemi, J.B. Clark, The Ce−Mg (Cerium-Magnesium) system, J. Phase Equilib. 9 (1988) 162–172.
[20] H. Okamoto, Mg-Nd, J. Phase Equilibria Diffus. 28 (2007) 405.
[21] S.M. Zhu, J.F. Nie, M.A. Gibson, M.A. Easton, P. Bakke, Microstructure and creep behaviour of high-pressure die-cast magnesium alloy AE44, Metall. Mater. Trans. A 43A (2012) 4137–4144.
[22] G. Pettersen, H. Westengen, R. Høier, O. Lohne, Microstructure of a pressure die cast magnesium–4wt.% aluminium alloy modified with rare earth additions, Mater. Sci. Eng. A 207 (1996) 115–120.
[23] A.A. Kaya, A review on developments in magnesium alloys, Front. Mater. 7 (2020) 198.
[24] I.P. Moreno, T.K. Nandy, J.W. Jones, J.E. Allison, T.M. Pollock, Microstructural characterization of a die-cast magnesium-rare earth alloy, Scr. Mater. 45 (2001) 1423–1429.
[25] S.M. Zhu, M.A. Gibson, M.A. Easton, J.F. Nie, The relationship between microstructure and creep resistance in die-cast magnesium–rare earth alloys, Scr. Mater. 63 (2010) 698–703.
[26] S.M. Zhu, C. Wong, M.J. Styles, T.B. Abbott, J.F. Nie, M.A. Easton, Revisiting the intermetallic phases in high-pressure die-cast Mg–4Al–4Ce and Mg–4Al–4La alloys, Mater. Charact. 156 (2019) 109839.
[27] C. Wong, M.J. Styles, S. Zhu, D. Qiu, S.D. McDonald, Y. Zhu, M.A. Gibson, T.B. Abbott, M.A. Easton, (Al,Mg)3La: a new phase in the Mg–Al–La system, Acta Cryst. B 74 (2018) 370–375.
[28] S.M. Zhu, T.B. Abbott, M.A. Gibson, J.F. Nie, M.A. Easton, Age hardening in die-cast Mg–Al–RE alloys due to minor Mn additions, Mater. Sci. Eng. A 656 (2016) 34–38.
[29] C. Su, D. Li, A.A. Luo, T. Ying, X. Zeng, Effect of solute atoms and second phases on the thermal conductivity of Mg-RE alloys: a quantitative study, J. Alloy. Compd. 747 (2018) 431–437.